Physics of Fluids

RESEARCH ARTICLE | OCTOBER 31 2023

# Virus spreading in cruiser cabin

Special Collection: Flow and the Virus

Konstantinos Ritos (Κωνσταντίνος Ρήτος) ; Dimitris Drikakis (Δημήτρης Δρικάκης) ; Ioannis W. Kokkinakis (Ιωάννης Κοκκινάκης)



*Physics of Fluids* 35, 103329 (2023)
https://doi.org/10.1063/5.0169992

# Virus spreading in cruiser cabin

Cite as: Phys. Fluids 35, 103329 (2023); doi: 10.1063/5.0169992
Submitted: 31 July 2023 · Accepted: 12 September 2023 ·
Published Online: 31 October 2023

View Online Export Citation CrossMark

Konstantinos Ritos (Κωνσταντίνος Ρήτος),[1,2,a] Dimitris Drikakis (Δημήτρης Δρικάκης),[2,b] and Ioannis W. Kokkinakis (Ιωάννης Κοκκινάκης)[2,c]

## AFFILIATIONS

[1]Department of Mechanical Engineering, University of Thessaly, Volos 38221, Greece
[2]Institute for Advanced Modeling and Simulation, University of Nicosia, Nicosia CY-2417, Cyprus

**Note:** This paper is part of the special topic, Flow and the Virus.
[a]Electronic mail: konritos@uth.gr
[b]Author to whom correspondence should be addressed: drikakis.d@unic.ac.cy
[c]Electronic mail: kokkinakis.i@unic.ac.cy

## ABSTRACT

This paper concerns virus droplet simulations in a typical cruiser's cabin. Effects of ventilation rates and positions of the coughing person were investigated. The study also emphasizes the importance of including evaporation models to simulate the process accurately. A higher ventilation rate is not always the best strategy to avoid the spread of airborne diseases, as saliva droplets can spread further at high ventilation rates. Regardless of the ventilation strategy, they evaporate faster than the room's air renewal. One should aim for minimum droplet spreading inside the cabin and different ventilation strategies for occupied cabins. The authors propose using ventilation systems at medium flow rates of around 120 $m^3$/h or three air changes per hour when a cabin is occupied. This value is also close to the recommended value of 108 $m^3$/h from the latest standard by the American Society of Heating, Refrigerating and Air-Conditioning Engineers. The suggested value minimizes droplet spreading while maintaining good ventilation, comfort, and energy consumption.



## I. INTRODUCTION

The recent COVID-19 pandemic with more than $750 \times 10^6$ confirmed cases and almost $7 \times 10^6$ deaths[1] motivated the scientific community to study the mechanisms of infection and the virus's ability to mutate quickly.[2] The scientific community produced computational frameworks to assess which parameters should be considered when making predictive tools for pandemic evolution.[3–7]

In addition, researchers performed studies of how droplets and nuclei expelled by infected individuals spread, potentially infecting others, and produced appropriate mitigation guidelines and strategies. For example, Dbouk and Drikakis[3,4,8–11] investigated several factors associated with distance, environmental conditions, face masks, and confined spaces. Verma *et al.*[12] studied experimentally with cough simulators the effectiveness of the different types of face masks, highlighting the importance of wearing a mask during a pandemic. Experimental and computational studies[9,13] visualized and estimated the spreading distance of a cough with and without a mask from individuals.

Moreover, many other studies are relevant to the present work and here we mention some. Pendar *et al.*[14] performed a series of simulations in a room under constant ventilation conditions and at various particle sizes and initial velocities, emulating sneezing and coughing droplets. They correlated the length and width of the total direct maximum reach of micro-droplets and provided advice on social distancing. Busco *et al.*[15] proposed a sneezing model for pressure variation at the mouth outlet through extensive experiments and simulations. They stated that during sneezing, the internal muscle contraction leads to sudden changes in pressure at the mouth outlet, which results in saliva droplets disperse in the surrounding environment. Their model captured the droplet spreading more accurately than conventional models, which usually led to more confined results.

As expected, a significant part of studies focused on high and long-time occupancy spaces with high risks of cross-infection, such as school classrooms. For example, Abuhegazy *et al.*[16] studied the spreading of saliva droplets and their surface deposition in a classroom under various conditions. They concluded that large particles drop on the ground or other surfaces in the room due to gravity, while most small particles exit through the ventilation outlet. They proposed the installation of transparent partitions on each student's desk during pandemic breakouts to reduce contaminant spreading.

Air purification in indoor spaces is important and recent studies discussed this issue.[17–21] For example, Dbouk *et al.*[17] investigated the limitations of air purifiers and proposed the optimal implementation of domestic air purifiers for eliminating airborne viruses in indoor spaces. Air purification and HEPA filters, which are supposed to capture more than 99% of particles, provide high ventilation rates with 50% fresh air and 50% filtered while delivering more than 20 air changes in the cabin.[22] However, the studies also showcased the inevitability of virus transmission when two persons are close.

Although aerosol transmission and ventilation configurations have been studied for cars[23,24] and buses,[25–27] research on this topic for cruise ships is limited. The transmission inside passenger cabins has been investigated only with mechanistic modeling[28] and data analysis from outbreaks.[29] A recent review on the transmission of COVID-19 in cruise ships[30] indicates that cabins of high occupancy have an increased transmission risk, without commenting on the cabin's ventilation system and how this could have affected the transmission. Computational fluid mechanics (CFD) studies with ventilation suggestions have been limited to small vessels.[31]

Furthermore, there have been contradicting arguments in the literature regarding the recirculation of possibly contaminated air and the ventilation rate efficiency in cruiser ships. Azimi *et al.*[28] suggested high ventilation rates in cruise ship cabins, but views differ among authors.[32–35]

The most recent standards and regulations on room safety regarding the airborne transmission of viruses focus on high rates of air exchanges.[36–38] This can be inefficient as large energy consumption is needed to maintain high air flow rates while comfort can be reduced due to the creation of strong air drafts.

The ASHRAE Standard[38,39] provides a formula for the minimum ventilation rate based on occupants and the surface area of a hotel bedroom $\dot{Q}_{outdoor-air} = R_p \times N_p + R_a \times A$, where $\dot{Q}_{outdoor-air}$ is the specified outdoor air that should be supplied in the room, $R_p$ is the required outdoor flow rate per person, $R_a$ is the required outdoor flow rate per unit area, and $A$ is the floor area of the room. The appropriate values for $R_p = 2.5\,\ell/(\mathrm{s}\quad \mathrm{person})$and $R_a = 2.5\,\ell/(\mathrm{s}\quad \mathrm{m}^2)$ are defined in the Standard[38,39] and lead to a value of $27\,\mathrm{m}^3/\mathrm{h}$ for the cabin presented here, assuming two occupants. The cruiser designers have proposed a stricter ventilation limit of $30\,\mathrm{m}^3/\mathrm{h}$ per room occupant, while the World Health Organization (WHO),[40] the European Federation of HVAC Associations,[41] and research studies[42] recommend $36\,\mathrm{m}^3/\mathrm{h}$ per person. The Federal Public Service (FPS) Health, Food Chain Safety and Environment of Belgium defined the minimum flow rate for their Standard A Level at a slightly higher value of $40\,\mathrm{m}^3/\mathrm{h}$ per person.[43]

Considering the above and that it is more likely that two people occupy a small cruiser cabin, our reference flow rate value is $60\,\mathrm{m}^3/\mathrm{h}$. The most recent CDC guidelines based on the draft of ASHRAE Standard 241–2023,[38] similarly by other studies,[44] propose a minimum of five air changes per hour (ACH), which translates to a flow rate of $200\,\mathrm{m}^3/\mathrm{h}$ for the cabin we investigate in this paper. The ASHRAE Standard 241–2023[38] recommends 15 l/s per occupant, which is equal to $108\,\mathrm{m}^3/\mathrm{h}$ for the studied cabin. In comparison, a typical home has less than 0.5 ACH based on CDC data, while this number reduces to 0.35 ACH based on the recommendation from ASHRAE Standard 62.2–2019.[45]

In this study, we examine a typical cruise ship cabin and how ventilation can affect the transmission of airborne viruses based on the guidelines from older (pre-COVID) and recent standards. Moreover, previous studies[10,46] have shown the effects of droplet evaporation, which, sometimes, is (incorrectly) omitted by researchers.[47] Here, we present results ranging from 1.5 to 15 ACH to capture all possible cases from poor/minimal ventilation up to exceeding the most recent recommendations. Droplets can spread up to five times more when utilizing high ventilation rates in the initial few seconds after a person has coughed. Overall, saliva droplets evaporate faster than the room's air renewal, regardless of the ventilation strategy. This highlights the importance of evaporation when modeling the saliva droplets spread. Moreover, we will show that the airflow rate has a nonlinear effect on droplet spreading.

The paper is organized as follows. Section II presents the methods and models used in the study. Section III presents the geometry and boundary conditions. The results are presented in Secs. IV and V. The conclusions drawn from this study are summarized in Sec. VI.

## II. SIMULATION METHODS

Ambient air conditions and other simulation parameters are shown in Table I, while saliva has been considered a Newtonian fluid with water properties. Although saliva is a complex fluid and varies from person to person, taking its viscosity close to that of water is a valid approximation.[48]

For the multiphase simulations, we consider a fluid mixture with a multicomponent gas (dry air and water vapor) and liquid water as Lagrangian particles. To achieve the values given in Table I, the gas mass fractions at the air inlets have been specified as 0.99207–dry air and 0.00793—water vapor, while liquid water is only inserted during the coughing event from the person's mouth.

The following items have been considered in the mass transfer and evaporation of airborne droplets from a coughing person:

1. The initial saliva speed and the duration of the cough.
2. The saliva droplet's initial size distribution at the onset of the coughing event.
3. The numerical modeling approach to capture the complex varying space and time scales, e.g., heat and mass transfer considerations, modeling of mass and phase changes due to droplet evaporation in interaction with the bulk flow field.

A fully developed flow is achieved after 60 s of simulation time. Human cough is imitated over 0.12 s. The velocity applied at the mouth during the cough is $u_x = 8.5$ m/s, as measured by Ref. 49. The initial total mass of the injected saliva into the domain is 7.7 mg, which agrees well with existing experimental measurements reported in the literature.[50,51] The simulation continues for another 20 s, at least, where more than 99.99% of the saliva droplets have evaporated in all cases studied here. During the initial 60 s, and after the coughing event, the air is expelled from the mouth with $V_{breath} = 0.1$ m/s.

Regarding the droplet's initial size distribution, we follow the well-documented and justified practice per Ref. 8. regarding the

**TABLE I.** Simulation conditions. The air changes per hour (ACH) varies depending on the flow rate of the ventilation system. The person's mouth is always considered as an inlet with the same relative humidity (RH) as the environment and the specified temperature.

| $T_\infty$ (°C) | $P_\infty$ (atm) | RH (%) | ACH |
|---|---|---|---|
| 20 | 1 | 55 | 1.5−15 |
| $T_{mouth}$ (°C) | $V_{cough}$ (m/s) | $V_{breath}$ (m/s) | Ejected saliva (mg) |
| 34 | 8.5 | 0.1 | 7.7 |

droplet's size distribution near the origin of ejection.[51] Based on the above, the size distribution imposed at the particle injector corresponds to the Rosin–Rammler distribution law,[52] also known as the Weibull distribution.[53] This is an appropriate distribution for dispensing water and water-like cloud droplets,[54] and its exact form is

$$f = \frac{n}{\bar{d}_p}\left(\frac{d_p}{\bar{d}_p}\right)^{n-1} e^{-(d_p/\bar{d}_p)^n}, \tag{1}$$

where $d_p$ is the saliva droplet diameter, $n = 8$ and $\bar{d}_p = 80\ \mu$m.

This study focuses on the effect of ventilation flow rates and a person's positioning in a cabin when the droplets' evaporation can occur. At the same time, the overall flow velocity is rather small (less than 2 m/s, except for the coughing event when the velocity increases for a small period to 8.5 m/s). We employ a compressible, unsteady multiphase solver with the Ranz–Marshall model applied for the Nusselt and Sherwood numbers.[55,56] All simulations have been performed with Star-CCM+ 2210.[57] We utilize the ideal gas law to express the density as a function of temperature and pressure in our calculations. The dynamic viscosity of air and water vapor is calculated based on the Sutherland's law. We use a second-order implicit temporal solver. A laminar multicomponent gas model allows us to add the different substances of the Eulerian fluid, i.e., air and water vapor (humidity), leading to a more accurate representation of the gas in the cabin. A segregated flow solver with secondary gradients and flow-boundary diffusion fluxes is activated. The linkage between the momentum and continuity equations is achieved with a predictor–corrector approach. Essentially, the solver uses a collocated variable arrangement and a Rhie-and-Chow-type pressure–velocity coupling combined with a SIMPLE-type algorithm. This solver can handle mildly compressible flows and low Rayleigh number natural convection, as in the cases studied here. Convection is solved with a second-order upwind scheme, which introduces linear interpolation of cell values on either side of the upstream or downstream face. A positivity rate limit of 0.2, necessary for compressible segregated solvers, controls the maximum allowable pressure correction update. Similarly, a second-order segregated fluid temperature model solves the total energy equation, with temperature as the solved variable. Enthalpy is calculated from temperature according to the equation of state. Two transport equations are solved sequentially with a second-order segregated species solver and, along with the global mass continuity, leading to updating the two mass fractions defining the mixture composition of the air in the cabin.

We have used the Venkatakrishnan limiter with second-order accuracy to reconstruct the gradients at the cell faces. The scale factor $a = min(a_f)$ for a cell that expresses the ratio of the limited and unlimited values is calculated based on the following equation:

$$a_f = (2r_f+1)/(r_f(2r_f+1)+1), \tag{2}$$

where $r_f = (\phi_f - \phi_0)/(max(\phi_0, \phi_{neighbors}) - \phi_0)$ and $\phi_f$ is the face value while $\phi_0$ is the cell centroid value.

We apply no-slip and adiabatic boundary conditions at all solid surfaces for the Eulerian model. The maximum time step used in the implicit temporal solver was 0.01 s, which was reduced to 0.5 ms during the coughing event.

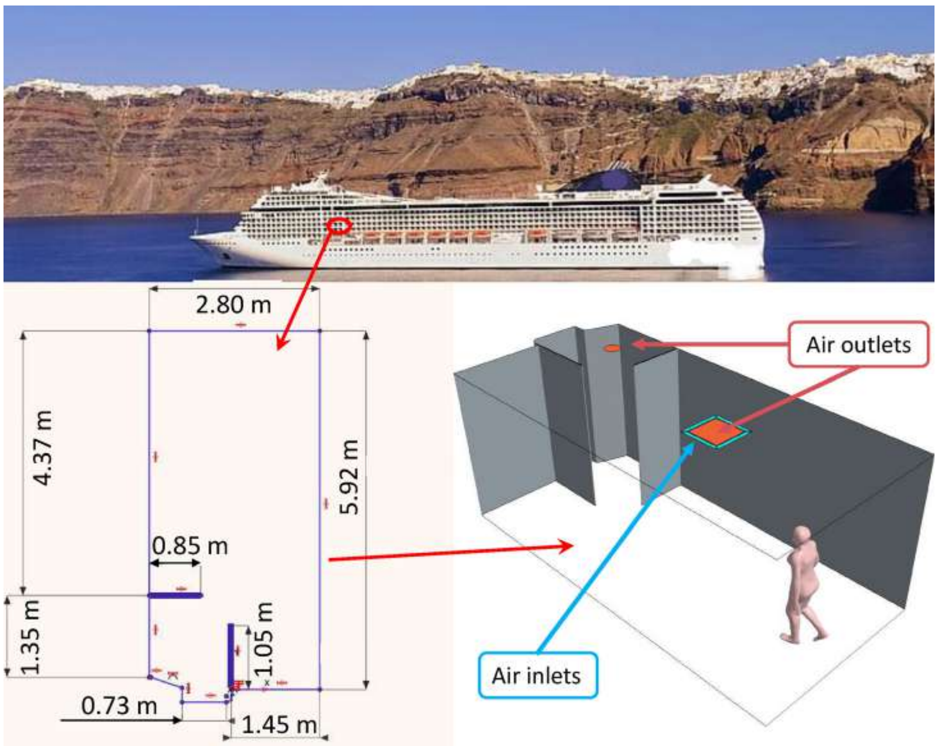


**FIG. 1.** Schematic representation of a representative cruiser ship cabin and the equivalent simulation domain.

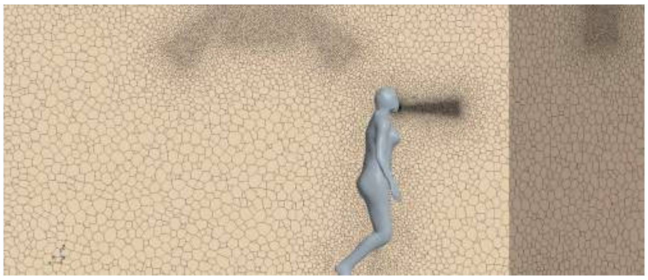

**FIG. 2.** Snapshot of the polyhedral mesh utilized in the simulations (case B) highlighting the areas of refinement.

The droplet's Lagrangian phase equations were discretized employing implicit numerical schemes at second order with two-way coupling and a quasi-steady evaporation model. Second-order temporal and spatial discretization of the governing equations was used in all production runs. In the Lagrangian framework, the equation of conservation of momentum for a liquid droplet of mass $m_d$ is given by

$$m_d \frac{d\mathbf{v}_d}{dt} = \mathbf{F}_d + \mathbf{F}_p + \mathbf{F}_v m + \mathbf{F}_g. \tag{3}$$

In this study, we calculate the drag ($\mathbf{F}_d$), pressure gradient ($\mathbf{F}_p$), and gravity ($\mathbf{F}_g = m_d g$) forces, while the virtual mass force ($\mathbf{F}_v m$) can be safely ignored for the particle sizes studied here.[14,16] The drag force calculates the force on a material particle due to its velocity relative to the continuous phase based on

$$F_d = \frac{1}{2} C_d \rho A_d |\mathbf{v}_s| \mathbf{v}_s, \tag{4}$$

where $C_d$ is the drag coefficient, $\mathbf{v}_s = \mathbf{v} - \mathbf{v}_d$ is the droplet slip velocity, and $A_d$ is the projected area of the droplet. The drag coefficient in the above-mentioned equation is a function of the small-scale flow features around individual particles. Resolving those features for thousands of particles is intractable from a computational efficiency perspective. It is common practice to obtain the drag coefficient from correlations, typically derived from experimental or theoretical studies. For the small liquid droplets in a viscous continuous phase, we consider the most appropriate correlation to be the Schiller–Naumann,[58] which is formulated as

$$C_d = \begin{cases} \dfrac{24}{Re_d}\left(1 + 0.15 Re_d^{0.687}\right), & \text{if } Re_d \le 10^3, \\ 0.44, & \text{if } Re_d > 10^3, \end{cases} \tag{5}$$

where $Re_d$ is the droplet Reynolds number. For the pressure gradient force, we do not need any correlation as it is based on the droplet's volume ($V_d$) and the static pressure of the continuous phase ($p_{static}$),

$$\mathbf{F}_p = -V_d \nabla p_{static}. \tag{6}$$

Droplet collision, atomization, and secondary breakup are not considered due to the low concentration of particles in the cabin.[59] A stick boundary condition is applied when droplets reach a solid surface, a common practice in the literature for this range of particle sizes.[16,47,59] The authors recognize that, in reality, some of the particles could be reflected on solid surfaces or reenter the air after deposition. However, their effect on our observations would be infinitesimal.

Droplets have a constant density equal to 997.561 kg/m$^3$, while the effect of the nonvolatile compounds, such as salt and lipids, on the size change during the evaporation of the droplets was ignored. The

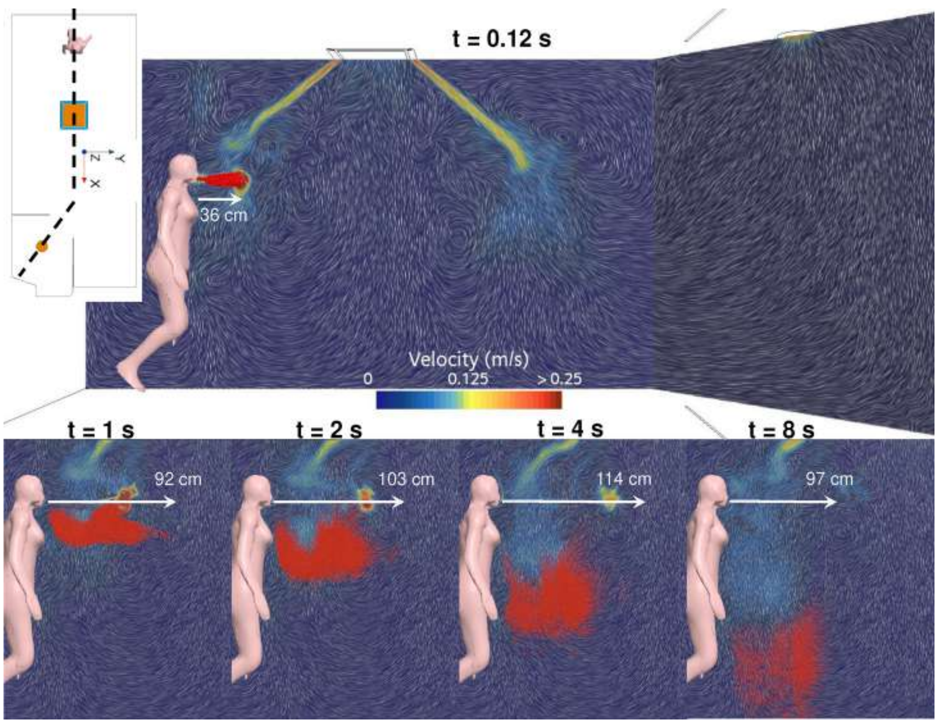


**FIG. 3.** Snapshots of the droplets and flow field at various instances for a volumetric flow rate of 60 m$^3$/h, CaseA60. The inset schematic is a top-down view of the cabin with the black dashed line indicating the location of the plane where the flowfield is illustrated.

latent heat of vaporization is calculated directly as a difference in the enthalpy of the gas and liquid states as follows:

$$L(T_d) = h_{vap}(T_d) - h_{liq}(T_d), \tag{7}$$

where $T_d$ is the droplet temperature, $h_{vap}(T_d)$, is the static enthalpy of the vapor component corresponding to the droplet material, evaluated at the droplet temperature, and $h_{liq}(T_d)$ is the static enthalpy of the droplet material, evaluated at the droplet temperature. The saturation pressure $p_{sat}$ is the pressure of each vapor component when in equilibrium with the corresponding liquid component and is a key material property. In this implementation, we use the Antoine equation, which is based on the logarithm of the ratio $p_{sat}/p_{atm}$ as we show in the following equation:[60]

$$ln(p_{sat}/p_{atm}) = 11.949 - 3978.205/(T_d - 39.801). \tag{8}$$

Four different flow rates for the air from the ventilation system and their effect on saliva droplet spreading and evaporation are examined. In addition, two positions of the coughing person, one at the far end of the room and one in the middle, are studied. The total computation time of a single case (80 s of simulation) was about 2.5 days, run in parallel over two Intel-Xeon Gold 6138 CPUs with 20 cores each at a frequency of 2 GHz. The incoming air is considered clean, i.e., free from contaminants, without specifying whether it is outdoor air or treated with filtered recirculated air. It is common practice that some ventilation systems use filtration and air treatment, i.e., UV radiation, ionization, etc., to reduce the concentration of infectious particles. Thus, they give an equivalent-ACH (eACH) as if outdoor air was introduced, now recognized by the latest ASHRAE standard.[38] However, devices that provide eACH for specific particles may not be effective against other contaminants, such as gases and vapors, and must be used appropriately.

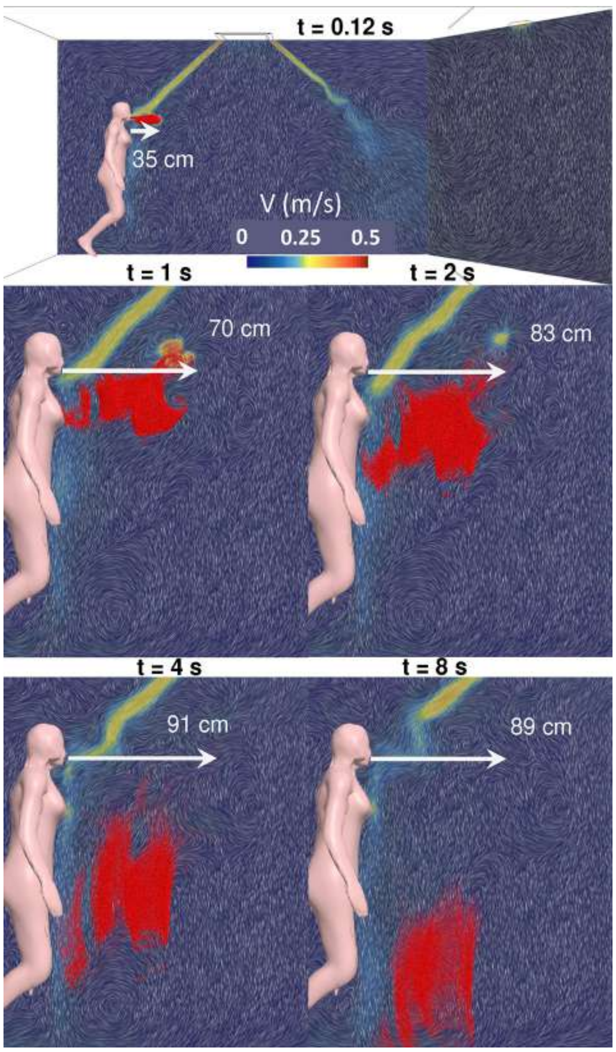


**FIG. 4.** Snapshots of the droplets and flow field at various instances for a volumetric flow rate of 120 $m^3$/h, CaseA120.

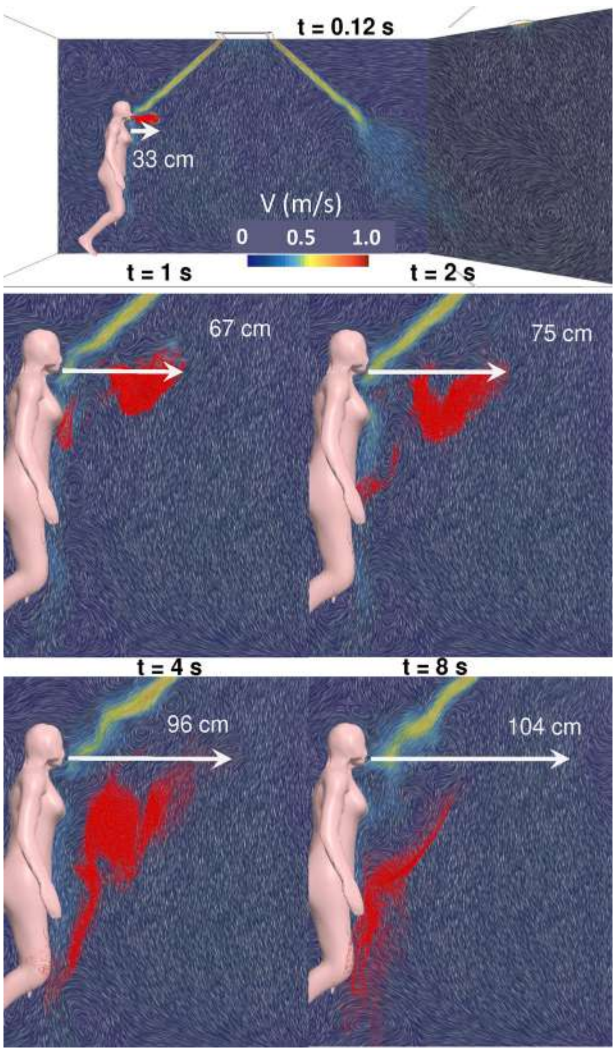


**FIG. 5.** Snapshots of the droplets and flow field at various instances for a volumetric flow rate of 240 $m^3$/h, CaseA240.

## III. CABIN GEOMETRY AND BOUNDARY CONDITIONS

In this study, we have chosen a representative cruiser cabin with the floor dimensions shown in Fig. 1. The cabin height is 2.4 m, with the overall deck height of the ship being 2.8 m. A standard air conditioning unit is placed at the cabin's center with a square outlet (□48 cm) and four rectangular inlets ($55 \times 5\,cm^2$ each) that expel air at an angle of 45°. The bathroom area has an additional circular outlet (∅25 cm).

The geometry has been meshed with polyhedral non-uniform cells ($\approx 0.6 \times 10^6$), with significant refinement in all inlet and outlet regions, where a conical refinement area is defined in each case. For example, at the mouth and up to a distance of 0.5 m in the streamwise direction, the cells have a maximum isotropic size of 4 mm compared to the overall targeted cell size of 4 cm. Enhanced quality triangles were used for the surface meshing method and five core mesh optimization cycles with a quality threshold of 0.6 for the entire mesh. A characteristic snapshot of the mesh is given in Fig. 2, where the refinement regions in front of the coughing person and the ventilation inlets and outlets are visible. The greatest volume change was 0.01 in less than 2% of the cells, while the mesh had 100% face validity. The maximum skewness angle was 86.5°. The choice of this mesh has been taken after conducting a mesh convergence study on main local and global flow parameters, like the cabin's average temperature ($T_{avg}$), relative humidity ($RH$), momentum, and mass conservation of the fluid. Furthermore, we have examined five different meshes on a similar case, from 74 000 cells up to more than $3.3 \times 10^6$. Employing the same meshing approach and refinement techniques, the chosen mesh of $\approx 0.6 \times 10^6$ polyhedral cells lead to a maximum difference of 5% when measuring the velocity at a random location in the simulation domain. At a second location, the error was less than 3% in air velocity, while $T_{avg}$ and $RH$ errors over the whole simulation domain were well below 1%. In addition, the error of the chosen mesh to the maximum and minimum pressure in the domain was also less than 0.8%. The coarsest mesh tested exhibited errors over 20% in velocity and 30% in pressure.

No-slip boundary conditions have been applied on all walls, the ceiling, the floor, and the person's body. Outlet boundary conditions with a specified mass flow rate have been applied in the Air outlets, shown in Fig. 1, with 1/3 of the flow directed to the bathroom outlet and the rest to the A/C outlet leading to a pressure balance in the cabin. The air inlets provide the overall targeted mass flow rate with the air blowing at an angle of 45°.

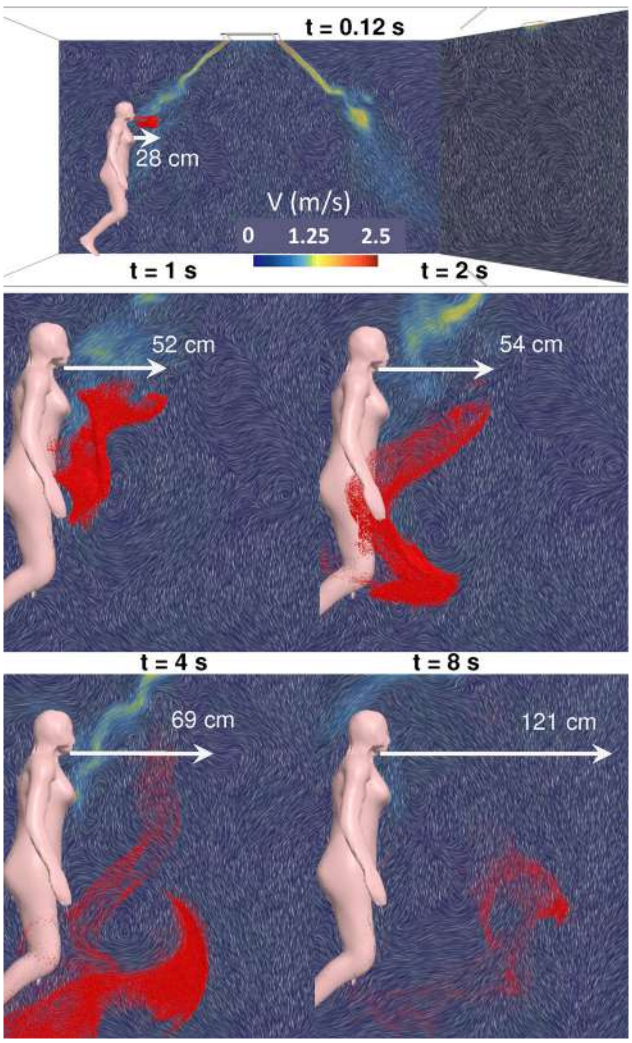


FIG. 6. Snapshots of the droplets and flow field at various instances for a volumetric flow rate of 600 $m^3$/h, CaseA600.

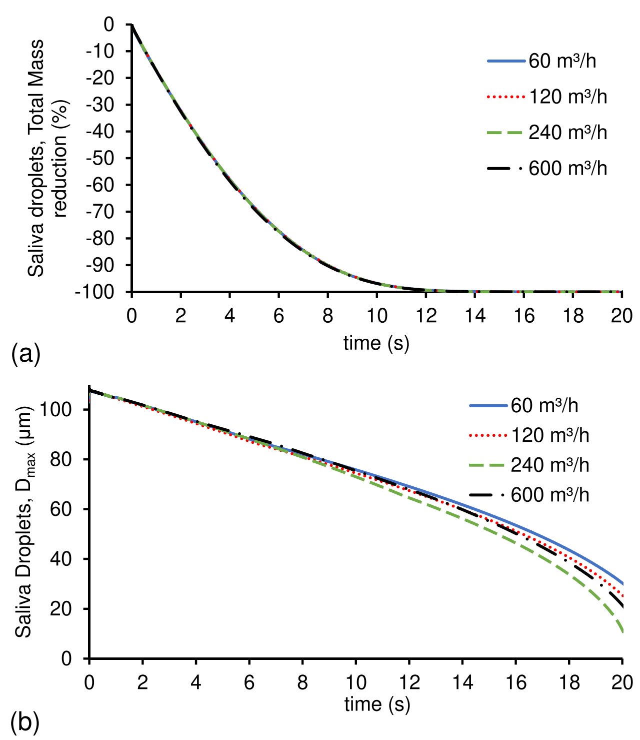


FIG. 7. (a) Total mass reduction of the droplets and (b) evolution of the maximum droplet diameter—case A.

## IV. VENTILATION FLOW RATE EFFECT

In the first case, we place the person close to the far end of the cabin and in the middle of the spanwise direction, as shown in Figs. 1 and 3. The height from the ground (at $z = 0$) to the mouth is 1.53 m, corresponding to real human dimensions. On further examining Fig. 3, we observe that saliva droplets have traveled less than 36 cm after the coughing event. At the same time, the flowfield in the room is smooth with an upward motion below the two outlets and overall very small air velocity. Saliva droplets travel quickly the first 91.5 cm away from the mouth of the person in the first second after the coughing event has started. In contrast, the maximum distance in the coughing direction is reached after only 4 s. In the last snapshot of Fig. 3 at 8 s after coughing, most of the droplets have either evaporated or settled below the waist height of the person.

Increasing the ventilation flow rate significantly affects the distance that the saliva droplets can travel (Figs. 4–6). During the initial 2 s, the droplets have traveled in the coughing direction (penetration) ∼20%, ∼27%, and ∼45% less than the reference case, as the flow rate increases to 120, 240, and 600 $m^3/h$, respectively. At 4 s, the distance reduction of the two higher flow rates decreases to ∼15% and ∼39%, respectively, while for $\dot{Q} = 120\,m^3/h$ (CaseA120), the distance reduction is the same as in previous times. At 8 s, when most of the droplets have evaporated, the two highest flow rates affect the droplets' penetration distance reduction. At the same time, CaseA120 showcases a distance reduction of ∼9% compared to the reference case.

The above-mentioned initial visual analysis of the results gives us the first indication that a higher ventilation flow rate will initially reduce the penetration distance of the droplets. Still, the trend can be reversed at later times. In combination with the findings of Fig. 7(a), where the evaporation rate (or mass reduction) of the droplets seems to be insensitive to the flow rate, one could quickly assume that increasing the ventilation over 120 $m^3/h$ would be an unnecessary cost with a probably added discomfort to the occupants of the cabin.

Cabins would contain furniture, electronic devices, and other personal items of the passenger not included in the present simulations. We have intentionally omitted the inclusion of those items because the employed air velocities are low, and the droplets will reach the floor before the airflow affects their circulation due to furniture. Thus, adding furniture and other objects will only increase the complexity of the meshing process without offering additional information or altering our conclusions. However, any particles deposited on the furniture may evaporate slower, depending on the furniture's material.

The evaporation process of the saliva droplets and its correlation with the ventilation flow rates have been further examined. The maximum droplet diameter ($D_{max}$) in Fig. 7(b) shows that the flow field velocity affects the evaporation process, particularly at later times ($t > 10$ s), where less than 3.5% of the initial total mass of saliva droplets is still present in all cases.

As expected, increasing the ventilation flow rate leads to faster evaporation except for the highest flow rate (CaseA600), where $D_{max}$ has a slower reduction than CaseA240. This is related to the room's overall flow field and that droplets fall quicker on the floor at higher ventilation rates, thus limiting evaporation under certain conditions. Similar observations can be made if we examine the mean diameter of the droplets (not shown here) 20 s after the coughing event, which reduces to 25, 20, 0 (complete evaporation), and 12 $\mu$m, respectively, for the four different flow rates. It should be underlined that 20 s after the coughing event, only an infinitesimal fraction of the initial saliva mass expelled in the air has not evaporated (less than 0.0001%) in all cases. The evaporation time of ∼20 s of the largest droplets is in-line with previous publications at a similar temperature and relative humidity conditions.[15,61–63]

After establishing that the ventilation flow rate minimizes the evaporation process, we focus on spreading the saliva droplets in the cabin. The trend on droplet spreading in the initial 8 s of the coughing event, discussed in Figs. 3–6, is also confirmed in Fig. 8(a). Specifically, CaseA120 has the lowest saliva droplet penetration at around 1 m

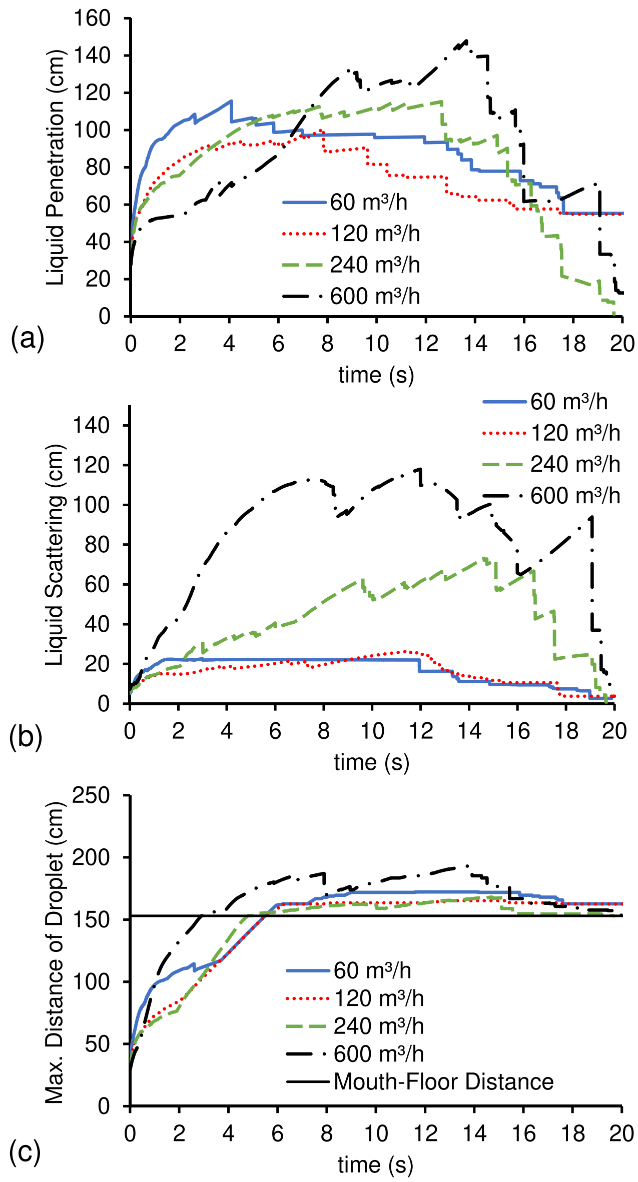


FIG. 8. Case A: (a) Maximum distance of droplets away from the mouth in the x direction (penetration), (b) maximum distance of droplets away from the mouth in the y direction (spanwise scattering), and (c) maximum distance of droplets away from the mouth (in 3D space). The floor is at 1.53 m (z direction).

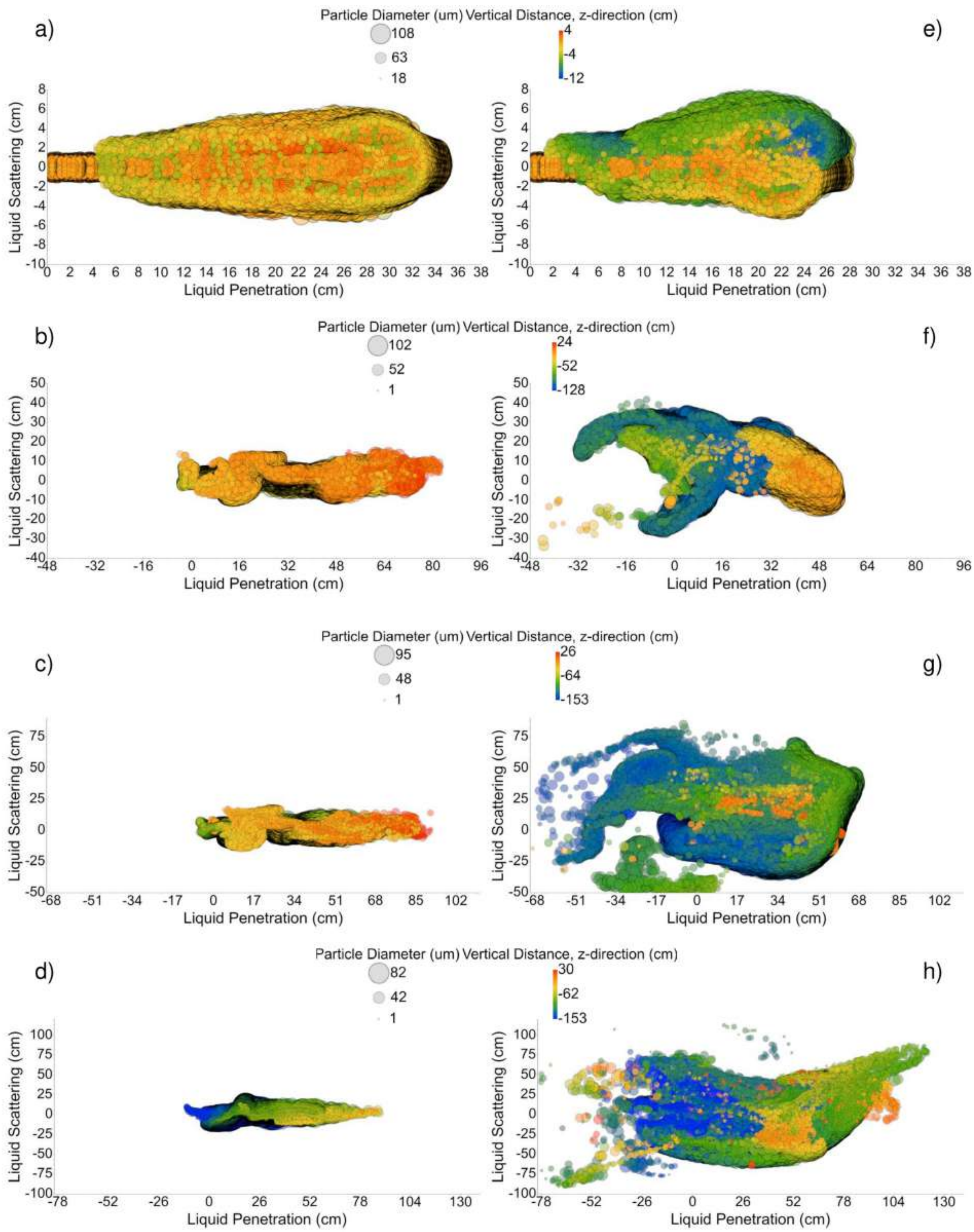


**FIG. 9.** Particle spreading in case A for two different flow rates, left column (a–d) 120 $m^3$/h and right column (e–h) 600 $m^3$/h at four different time instances: 0.12 (a and e), 2 (b and f), 4 (c and g), and 8 s (d and h).

away from the infected person. The high flow rate case (CaseA600) is also interesting because although it has the highest penetration value of around 1.5 m, this is observed around 15 s after the coughing event when only traces of the initial saliva mass can be found, and the maximum droplet size is below 60 $\mu$m.

Examining the spanwise scattering of the saliva droplets, which is not shown in Figs. 3–6, Fig. 8(b) shows that the high flow rate cases (CaseA240 and CaseA600) scatter saliva droplets around the infected person at distances more than three times compared to the reference case. CaseA120 has almost the same scattering pattern as the reference case.

Furthermore, Fig. 8(c) shows the total maximum distance traveled by a saliva droplet at each instance. The graph also includes the mouth-to-floor distance, as most droplets will fall due to the combined effect of gravity and induced flow by the ventilation system. Saliva droplets reach the ground in less than 4 s in CaseA600 [Figs. 8(c) and 6]. In the other cases studied here, saliva droplets seem to take a similar time to reach the ground. The initial high total distance observed in CaseA60 is attributed to the penetration distance, as the ventilation system is not strong enough to reduce the distance traveled by the droplets in the streamwise direction.

Dbouk and Drikakis[8] studied the penetration distance of saliva droplets for different wind velocities. They found maximum penetration distances of about 1.6 m for no wind and 6 m for a 4 km/h wind. In case A of our study, the air blown from the A/C unit can oppose the penetration of the particles, while in case B, there is a positive component on the air velocity. In all cases, the maximum recorded air velocity at the penetration direction is less than 0.6 m/s. Based on the above, we expect our penetration distances to be around the 1.6 m reported value and, in any case, much less than 6 m. This expectation is verified through the results of this study, where the reported distances are between 1 and 2.7 m. Focusing on case B and the two lower values of A/C flow rate, we can directly compare the reported values with those from the literature with no wind speed and find them within a comparable range. Pendar[14] also give a maximum distance of less than 1.5 m for droplets with an average diameter of 140 $\mu$m for the same temperatures as in our study.

From the above-mentioned results and accompanying discussion, it becomes evident that the appropriate ventilation rate can significantly influence the reduction of infected saliva droplets spreading in an internal space. For the specific cabin geometry, conditions and placement of the coughing person, the optimum flow rate is around 120 $\mu^3$/h, which can manage to contain saliva droplets in a small area around the infected person, while both higher and lower flow rates can have the opposite effect.

Focusing on the spreading of the saliva droplets, we make a more detailed comparison between the optimum flow rate of 120 $\mu^3$/h, from the cases examined and the maximum one of 600 m$^3$/h. In Fig. 9, we present the spatiotemporal evolution of the saliva cloud from the end of the coughing event up to 8 s later when most of the droplets have either evaporated, only ∼10% of the initial mass is still active in the computational domain or have settled on the floor of the cabin. The circles' size in the graph reflects the diameter of each droplet, while the color indicates the vertical distance from the ground, with zero being the height of the mouth and 153 cm is the floor. In case A, the airflow direction from the A/C unit tends to push the saliva cloud backwards and toward the floor. This becomes evident when comparing Fig. 9(a) with reffig:spreadAe, where in the latter, due to the very high flow rate, the droplets have both smaller penetration and lower elevation, which is clearly shown by the high number of droplets having a blue or green color. The shape of the saliva cloud is more symmetrical in the lower flow rate case compared to the higher flow rate case, as it is less affected by the air stream produced by the A/C unit. The distribution of sizes in each cloud at this initial stage is quite uniform.

At a later stage, 2 s after initiating the coughing event, the droplet clouds have evolved, taking remarkably different paths. In the lower A/C flow rate case [Fig. 9(b)], the saliva droplets form a more coherent and elongated cloud with minimal scattering. In addition, a significant amount of the droplets remains at a distance greater than 1 m from the floor, with some droplets at the front of the saliva cloud being elevated

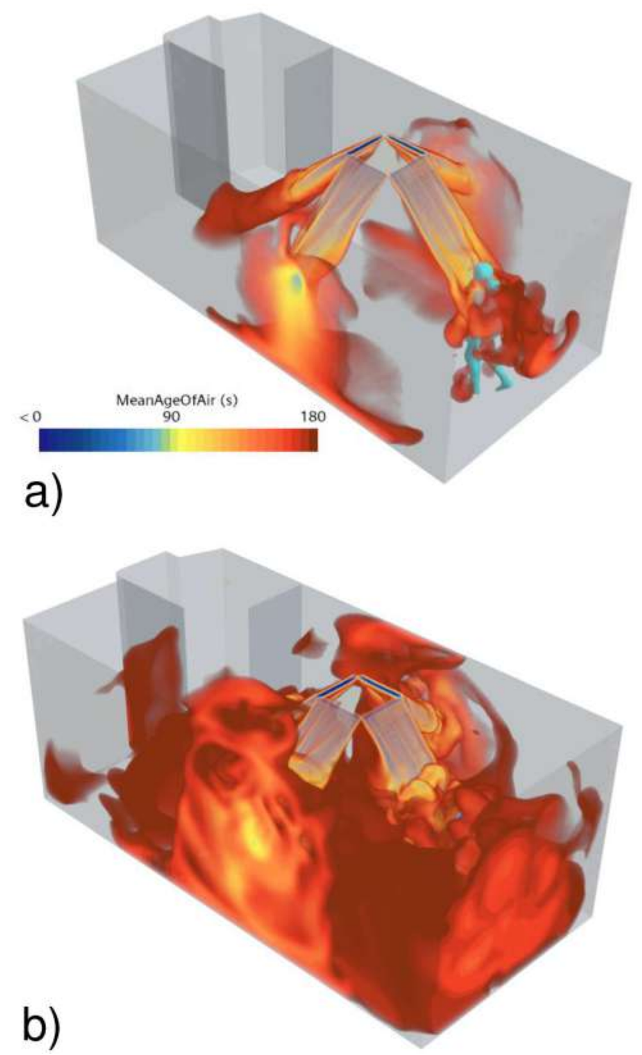


**FIG. 10.** Comparison of air refreshment after 3 min of ventilation for two different rates: (a) $\dot{Q} = 60$ and (b) $\dot{Q} = 120$ m$^3$/h. At the visualized flow rates, the cabin air is refreshed 1.5 and 3 times per hour. Colored regions show air that has an age of less than 3 min.

over the mouth height. The cloud front primarily consists of medium and small droplets, with the latter having a higher elevation, as expected. Larger sized droplets seem to concentrate around the middle of the saliva cloud and closer to the floor, as expected due to the gravitational forces. Moving to the high flow rate case [Fig. 9(f)], our observations are noticeably different. The saliva cloud has scattered to significantly greater distances, and many droplets have moved behind the person due to the strong air stream coming from the A/C unit. Interestingly, the cloud front has maintained a distinct higher elevation, over 1 m from the cabin's floor, while the saliva cloud's middle section is only ~30 cm away from it. We can also observe a few droplets detached from the cloud body and moved further away backwards and in the y direction (spanwise scattering). Similarly, smaller droplets have a higher elevation, but in this case, all droplets are below the mouth height. Larger droplets also seem to concentrate in the middle section of the saliva cloud.

In the third row of images [Figs. 9(c) and 9(g)], we can observe the evolution of the saliva cloud shape. In the low flow rate case, the saliva cloud looks very similar to the one 2 s earlier, with the main difference being the overall size reduction due to evaporation. Another observation we can make is that the droplets have more distinct stratification depending on their size, with smaller droplets ($<20\,\mu$m) being close to the mouth height and those at the cloud front being even higher. As the droplet size increases, the droplet elevation decreases, with the biggest droplets ($>50\,\mu$m) being less than 1 m from the cabin floor. At the same time instance, the droplet cloud in the high flow rate case [Fig. 9(g)] has expanded in all directions. Individual small and medium droplets ($<50\,\mu$m) can be observed more than 60 cm behind the coughing person and more than 70 cm in the spanwise direction. Close to the front of the droplet cloud, there are several very small droplets ($<10\,\mu$m) that retain a high elevation close to the mouth height. However, most of the droplets at the front of the saliva cloud are around 50 cm from the ground, while the majority of the rest of the droplets have already reached the cabin's floor or are very close to it.

At the last instance of 8 s, the saliva cloud from the low flow rate case retains its overall shape with a further reduction in size due to evaporation [Fig. 9(d)]. Most droplets close to the coughing person have settled on the floor, while those further away are still suspended in the region below the waist and a few centimeters above the ground. At the higher flow rate case [Fig. 9(h)], many droplets have settled on the ground; however, strong re-circulation air streams from the A/C unit have spread individual droplets further away at distances exceeding 1 m and also the saliva cloud seems to have maintained its elevation, while some droplets have even gain height compared to the previous time instance. It should be noted that at this last time instance, some droplets are at heights over 30 cm from the mouth height, even higher than any previous time, indicating the effect of the strong secondary air streams created by the ventilation system. The above-mentioned analysis strengthens our previous conclusions and observations that high ventilation flow rates create air streams that extend droplet spreading. In addition, here, we unveil that a secondary air stream, in the case of high flow rates, can levitate droplets from low heights to ones above the



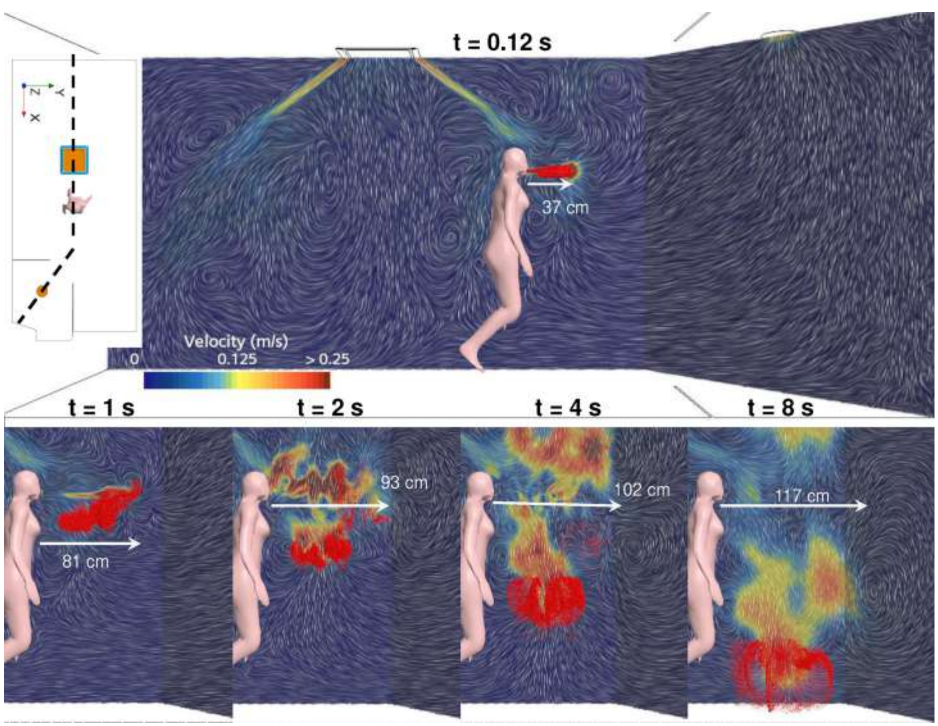


**FIG. 11.** Case B—snapshots of the droplets and flow field at various instances for a volumetric flow rate of 60 $m^3$/h, CaseB60. The inset schematic is a top-down view of the cabin with the black dashed line indicating the plane's location where the flowfield is illustrated.

coughing person's mouth and extend their suspension and spreading in the air.

It is also interesting to compare how much air has been renewed after 3 min from the coughing event when all saliva droplets would have completely evaporated. Figure 10 shows that the reference flow rate of 60 $m^3$/h refreshes only a small fraction of the cabin's air, and it would need around 40 min to completely refresh the cabin air fully, having an ACH of 1.5. In comparison, the ventilation rate minimizing droplet spreading (CaseA120) has refreshed a significant part of the cabin's air volume. However, there are still regions where fresh air has not reached yet. Even CaseA600 with an ACH of 15 would need an order of magnitude more time (4 min) to completely refresh the cabin's air than when saliva droplets evaporate (20 s). So, in that case, the infection could be attributed to fomite rather than airborne transmission.

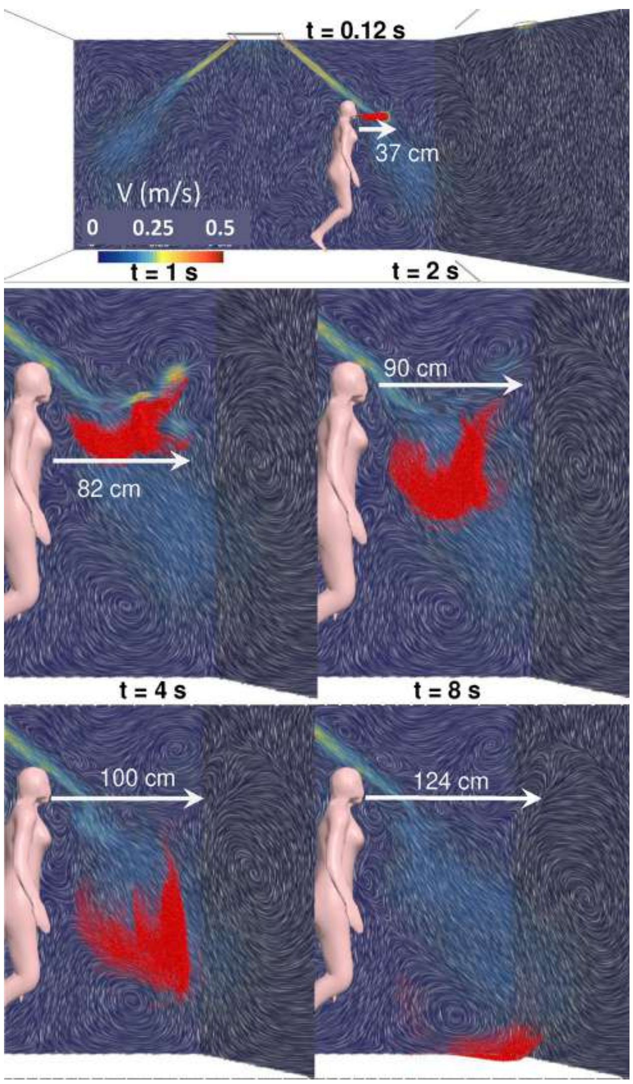


**FIG. 12.** Case B—snapshots of the droplets and flow field at various instances for a volumetric flow rate of 120 $m^3$/h, CaseB120.

## V. PERSON POSITIONING EFFECT

Next, we investigate the effect of moving the coughing person closer to the cabin's door and bathroom while maintaining all other parameters the same as before. In this situation, we can consider someone walking toward the bathroom while the coughing event initiates. As we will discuss in the analysis of the results below, although the air stream from the ventilation system is coming from a different direction (see Fig. 11), the overall conclusions will not differ from our previous observations.

The air from the ventilation system is blowing from behind and over the head of the coughing person in all Cases B. This has a minimal effect of less than 3% at the penetration distance of saliva droplets at the end of the coughing event with our reference flow rate of 60 $m^3$/h (cf. Figs. 3 and 11). Interestingly, the particles travel around 10% less

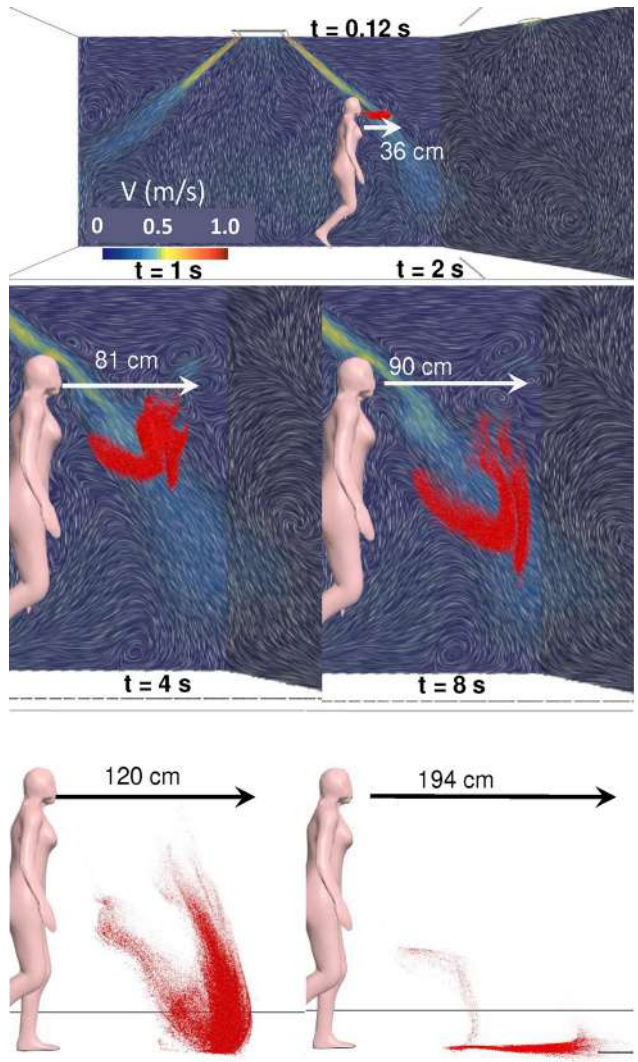


**FIG. 13.** Case B—snapshots of the droplets and flow field at various instances for a volumetric flow rate of 240 $m^3$/h, CaseB240. The flow field plane is not visualized at $t = 8$ s to highlight the spreading of saliva droplets.

in the axial direction (penetration) during the first 4 s than CaseA60, although one would expect the opposite effect by observing the airstream direction. At $t = 8$ s, saliva droplets have penetrated the cabin air volume by 20% than CaseA60.

At higher ventilation rates, all of cases B (Figs. 12–14) exhibit higher penetration values compared to their counterpart case A (from 10% at early stages up to 85% at the $t = 8$ s point), as expected. From the visual inspection of cases B, the effect of the ventilation airstream on the spreading direction of the saliva droplets is more pronounced. Especially in CaseB120 and CaseB240, the droplet cloud is carried away by the airstream diagonally away from the coughing person toward the floor. At the highest ventilation rate of 600 $m^3$/h, the particles move faster in the z direction toward the floor. At $t = 8$, the penetration distance is greater than 2 m, highlighting the inadequacy of the proposed social distancing during the COVID-19 pandemic, especially under conditions with high, but not extreme, ventilation rates.

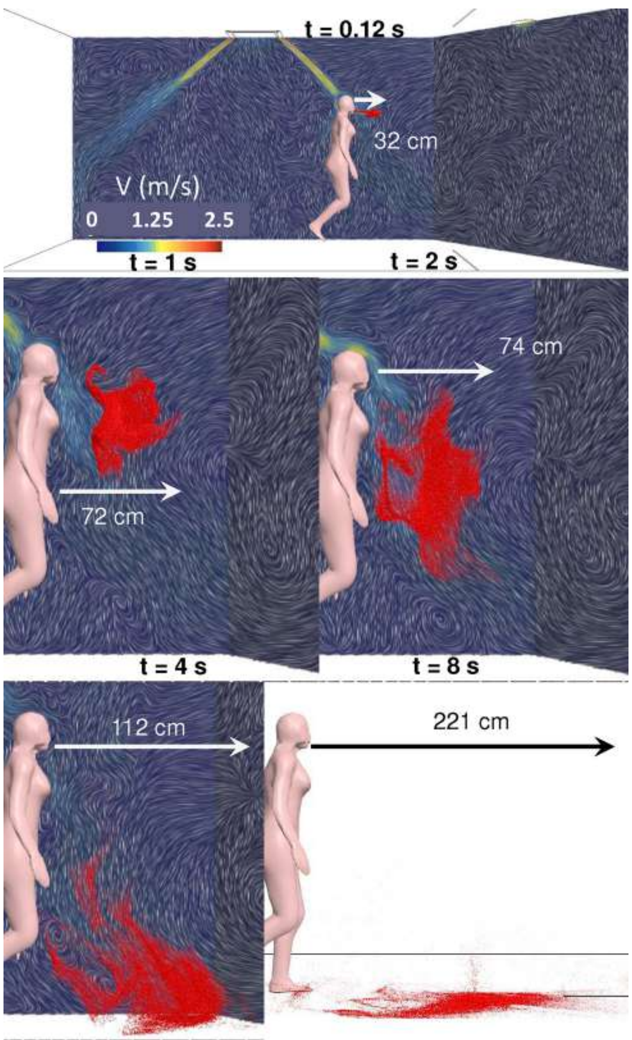


**FIG. 14.** Case B —snapshots of the droplets and flow field at various instances for a volumetric flow rate of 600 $m^3$/h, CaseB600. The flow field plane is not visualized at $t = 8$ s to highlight the spreading of saliva droplets.

Up to this point, our main conclusions do not alter, independently of the position of the coughing person. A higher ventilation flow rate will initially reduce the penetration distance of the droplets, but the trend can be reversed later. The evaporation rates in case B (Fig. 15) have similar trends except for the reference flow rate. In this instance, mass reduction is slightly slower at the lowest ventilation rate.

The overall mass and droplet diameter reduction is faster in case B, although the difference is small, and we expect such differences as the coughing person moves in the cabin. For completeness, we report here the mean diameter of the droplets for case B 20 s after the coughing event, which reduces to 14.5, 14, 26, and 12 $\mu$m, respectively, for the four different flow rates. Similarly, in case A 20 s after the coughing event, only an infinitesimal fraction of the initial saliva mass expelled in the air has not evaporated (<0.0001%) in all cases.

Finally, we want to examine if our conclusions on saliva droplets spreading in the cabin would be different between cases A and B. Figure 8(a) shows that droplets can travel at distances exceeding 2.5 m at the highest ventilation rate. Compared with case A, all flow rates show higher penetration values, as expected due to the airstream pattern. Moreover, the droplets fall quicker to the floor with higher ventilation rates, as we can observe in Fig. 16(c). From the results here, it is confirmed that there is an optimum ventilation rate, which is CaseB120, that has both the lowest penetration and scattering values (see Fig. 16) among the examined ventilation rates.

The final detailed comparison between two flow rates, 120 and 600 $m^3$/h, is made similarly to case A. Moreover, we comment on similarities and differences between the two cases and the effect of the

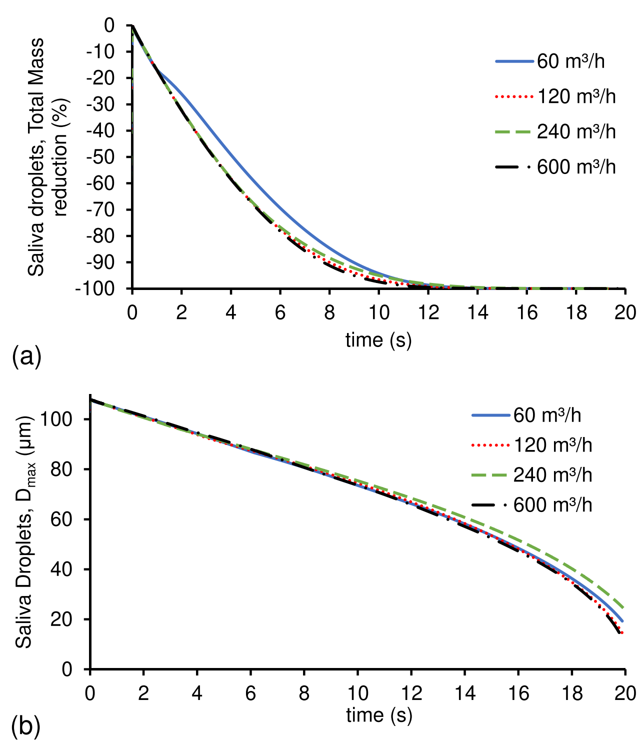


**FIG. 15.** (a) Total mass reduction of the droplets and (b) evolution of the maximum droplet diameter—case B.

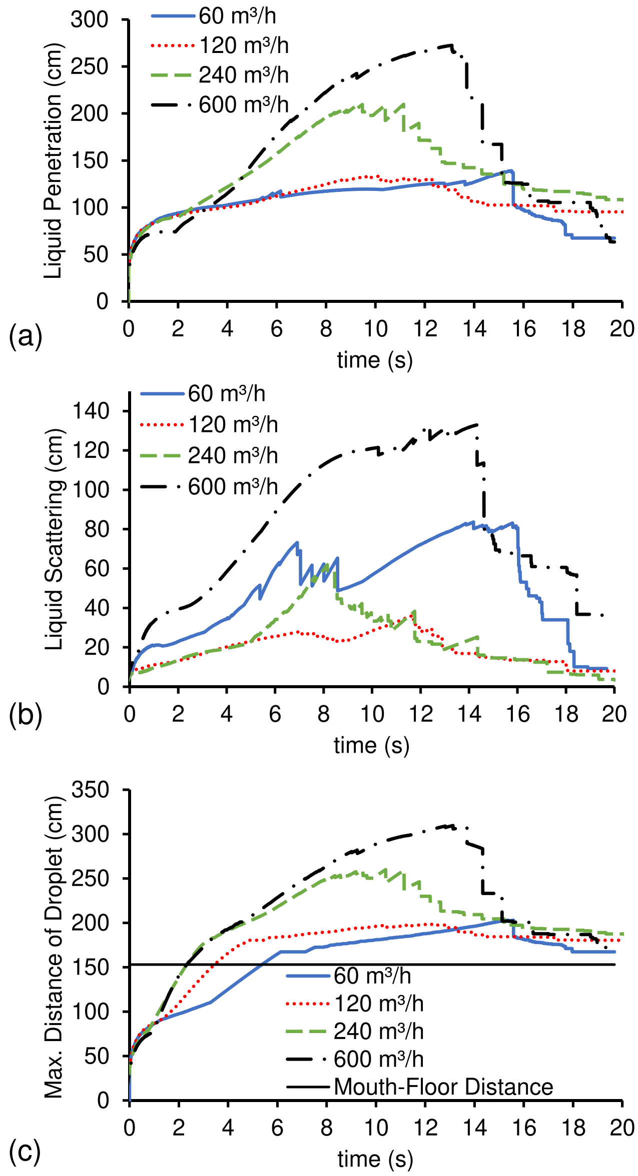


**FIG. 16.** (a) Maximum distance of droplets away from the mouth at the x direction (penetration), (b) maximum distance of droplets away from the mouth at the y direction (spanwise scattering), and (c) maximum distance of droplets away from the mouth (in 3D space, xyz direction). The floor is 1.53 m at the z direction—case B.

person's positioning or ventilation air-stream direction. In Fig. 17, we present the spatiotemporal evolution of the saliva cloud from the end of the coughing event up to 8 s, similarly to Fig. 9. The circles' size in the graph reflects the diameter of each droplet, while the color indicates the vertical distance from the ground, with zero being the height of the mouth and 153 cm being the floor. In this case, the airflow direction from the A/C unit tends to push the saliva cloud toward the floor. The overall shape of the saliva cloud with optimum flow rate ventilation [Fig. 17(a)] is similar to case A [see Fig. 9(a)], with the difference of higher penetration, as the front of the saliva cloud has reached further distances, in the case of high ventilation rates [Fig. 17(e)] the saliva cloud is quite asymmetrical and it has not moved as far as the lower flow rate case, as one would expect. This could be due to recirculations and secondary air streams developing in front of the coughing person's face, which can be observed in Fig. 14.

At later stages, the saliva cloud moves forward, reaching a penetration of ∼120 cm and toward the floor while it shrinks for the optimum flow rate of 120 $m^3/s$ [see Figs. 17(b) and 17(d)]. In contrast, the saliva cloud in the high flow rate case spreads and expands while it also breaks into smaller droplet clouds, highly affected by the secondary air streams developed [see Figs. 17(e) and 17(h)]. Large droplets quickly settle on the floor, especially at high ventilation rates, while medium and small droplets tend to spread more and retain their elevation longer. This can be explained as those smaller droplets can be easily drifted and affected by various secondary air streams, which are much stronger in this higher flow rate case.

Moving to the last instance of 8 s, the saliva cloud from the low flow rate case [Fig. 17(d)] is much more coherent compared to the high flow rate case [Fig. 9(h)]. Most of the droplets have reached the cabin's floor at both flow rates. In addition, some small droplets near the coughing person's body have retained an elevation of ∼1 m above the cabin's floor. At the lower flow rate examined here, droplets at the front of the saliva cloud also retain a significant elevation compared to the high ventilation rate case. Finally, comparing the saliva cloud spreading and pattern between the two different positions of the coughing person and at high ventilation rates, we can observe that in case B, recirculations and secondary air streams affect the early instances (0.12–4 s) primarily, while in case A they had a strong effect even at the latest time instance where they elevate droplets at heights over the mouth of the coughing person.

Our main conclusion from case A, i.e., the optimum ventilation rate is around 120 $m^3/h$, is strengthened and remains valid after examining the results from case B. Using this ventilation rate, it is possible to confine saliva droplets in a small area around the infected person. We do not expect other ventilation conditions, such as temperature and relative humidity, to alter our conclusions and findings. The risk could be mitigated at other flow rates if the cabin geometry is altered.

## VI. CONCLUSIONS

A typical cruiser's cabin was considered, and virus droplet simulations were performed for several ventilation rates covering ACH values from 1.5 to 15 and two different positions of the coughing person. The study's results reveal that a higher ventilation rate is not always the best strategy to avoid spreading airborne diseases. It should be pointed out here that proper ventilation, which leads to quick desiccation, has a detrimental effect on the viability of Gram-negative bacteria, such as *E. coli*.[64] However, complete evaporation of the saliva droplets may not necessarily mean that all viruses[65] or bacteria[64] become instantly inactive. Therefore, we should aim at minimum droplet spreading inside the cabin and different ventilation strategies for occupied cabins.

Given the results presented in this study, we propose using ventilation systems at medium flow rates of around 120 $m^3/h$ or 3 ACH when a cabin is occupied. This is close to the recommended value of 108 $m^3/h$ from the latest Standard by ASHRAE on the Control of Infectious Diseases.[38] It is also around double the proposed flow rate from recent, established standards, and regulations[39–41,43] but almost half to what the latest guidelines from CDC[37] suggested. Our main argument for the proposed value is the necessity to minimize droplet

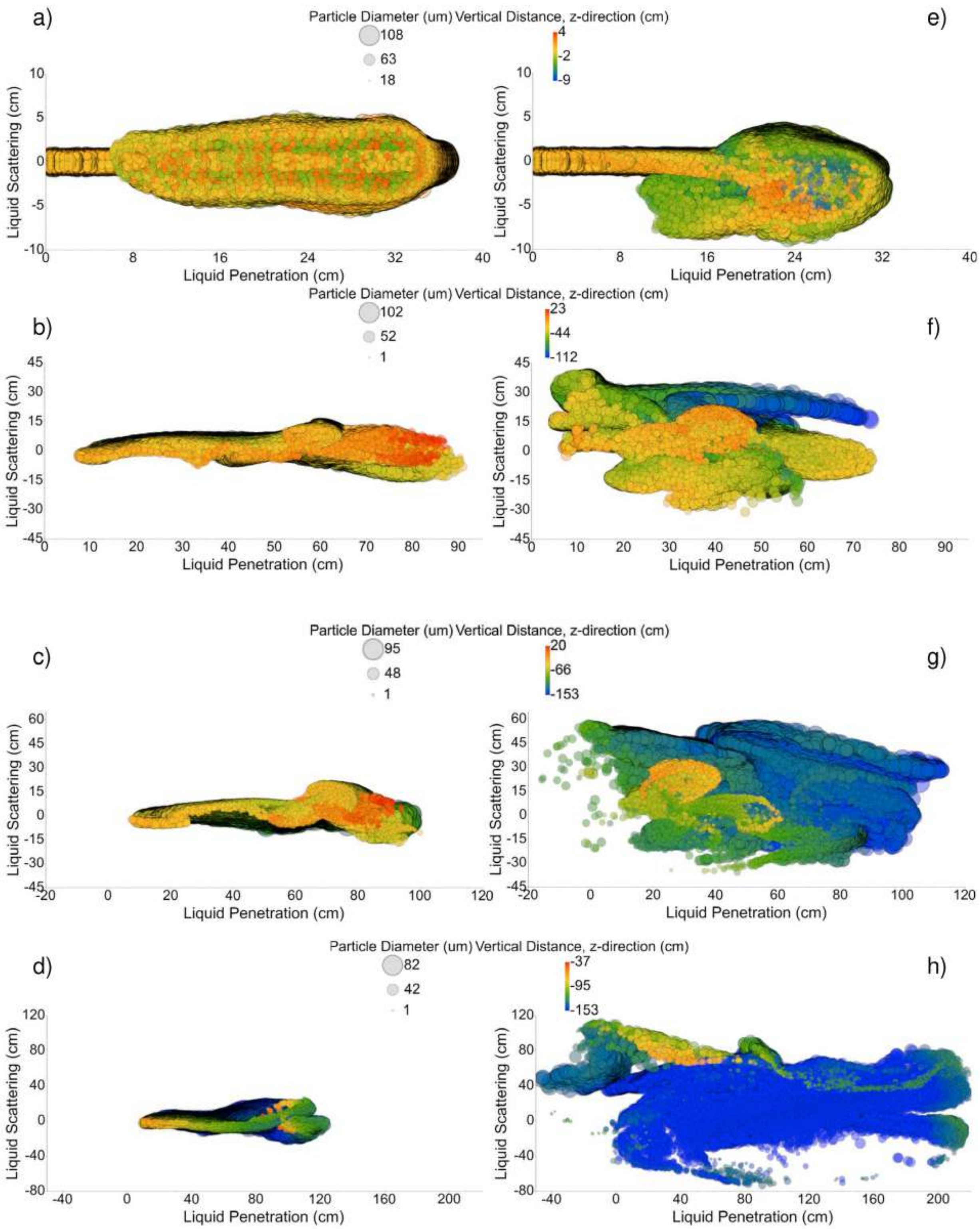


**FIG. 17.** Particle spreading in case B for two different flow rates: left column (a–d) 120 $m^3/h$ and right column (e–h) 600 $m^3/h$ at four different time instances: 0.12 (a and e), 2 (b and f), 4 (c and g), and 8 s (d and h).

spreading while maintaining good ventilation levels, comfort, and energy consumption, which seems to align with the ASHRAE 241–2023 Standard.[38] Moreover, the present work highlights how computational fluid dynamics can complement and improve ventilation standards and reduction in airborne infection transmission, a necessity underlined in the ASHRAE 241–2023.[38]

The ventilation rate could increase to 600 $m^3$/h or 15 ACH for 12 min after the room has been vacated before switching it off or reducing it to a minimum selected value. In this way, contaminated droplets would spread at a limited distance from the infected person while the air would be completely refreshed for the next occupants. The same minimum time of 12 min can also be proposed as a clearance wait time for similar-sized rooms with a minimum of 15 ACH. This is close to the proposed value by the CDC on Guidelines for Environmental Infection Control in Healthcare Facilities to remove 99% of airborne contaminant, assuming perfect air mixing within the room. Finally, keeping the ventilation rate at the proposed values benefits lower energy consumption and better comfort conditions for the occupants compared to higher ventilation rates.

## ACKNOWLEDGMENTS

This paper was supported by the European Union's Horizon Europe Research and Innovation Actions programme (Grant No. 101069937), project name: HS4U (HEALTHY SHIP 4U). The views and opinions expressed are those of the author(s) only and do not necessarily reflect those of the European Union or the European Climate, Infrastructure, and Environment Executive Agency. Neither the European Union nor the granting authority can be held responsible for them. The cabin image is courtesy of Celestyal Cruises. We thank Mr. Kostas Synodinos and Mr. Chrysanthos Chrysanthou for providing the drawing of the Celestyal cruiser cabin.

## AUTHOR DECLARATIONS

### Conflict of Interest

The authors have no conflicts to disclose.

### Author Contributions

**Konstantinos Ritos:** Conceptualization (equal); Data curation (lead); Formal analysis (equal); Investigation (lead); Methodology (equal); Software (lead); Validation (lead); Visualization (lead); Writing – original draft (lead); Writing – review & editing (equal). **Dimitris Drikakis:** Conceptualization (lead); Formal analysis (equal); Funding acquisition (lead); Investigation (equal); Methodology (equal); Project administration (lead); Resources (equal); Supervision (lead); Validation (supporting); Visualization (supporting); Writing – original draft (equal); Writing – review & editing (equal). **Ioannis William Kokkinakis:** Formal analysis (supporting); Investigation (supporting); Methodology (supporting); Software (supporting); Validation (supporting); Visualization (supporting); Writing – review & editing (supporting).

## DATA AVAILABILITY

The data that support the findings of this study are available from the corresponding author upon reasonable request.

## REFERENCES


[1] WHO. *WHO Coronavirus (Covid-19) Dashboard* (World Health Organization, 2023).

[2] D. Jamison, S. Anand Narayanan, N. Trovão, J. W. Guarnieri, M. J. Topper, P. M. Moraes-Vieira, V. Zaksas, K. K. Singh, E. S. Wurtele, and A. Beheshti, "A comprehensive SARS-CoV-2 and Covid-19 review. Part 1: Intracellular overdrive for SARS-CoV-2 infection," Eur. J. Hum. Genet. **30**, 889 (2022).

[3] T. Dbouk and D. Drikakis, "Correcting pandemic data analysis through environmental fluid dynamics," Phys. Fluids **33**, 067116 (2021).

[4] T. Dbouk and D. Drikakis, "Fluid dynamics and epidemiology: Seasonality and transmission dynamics," Phys. Fluids **33**, 021901 (2021).

[5] N. Christakis, M. Politis, P. Tirchas, M. Achladianakis, E. Avgenikou, C. Matthaiou, M. Kalykaki, A. Kyriakaki, P. Paraschis, E. Pilios, and G. Kossioris, "Covid-liberty, a machine learning computational framework for the study of the Covid-19 pandemic in Europe. Part 1: Building of an artificial neural network and analysis and parametrization of key factors which influence the spread of the virus," Int. J. Neural Netw. Adv. Appl. **8**, 12–26 (2021).

[6] N. Christakis, P. Tirchas, M. Politis, M. Achladianakis, E. Avgenikou, and G. Kossioris, "Covid-liberty, a machine learning computational framework for the study of the Covid-19 pandemic in Europe. Part 2: Setting up the framework with ensemble modeling," Int. J. Neural Netw. Adv. Appl. **8**, 27–42 (2021).

[7] M. Khan and A. Atangana, "Mathematical modeling and analysis of Covid-19: A study of new variant omicron," Physica A **599**, 127452 (2022).

[8] T. Dbouk and D. Drikakis, "On coughing and airborne droplet transmission to humans," Phys. Fluids **32**, 053310 (2020).

[9] T. Dbouk and D. Drikakis, "On respiratory droplets and face masks," Phys. Fluids **32**, 063303 (2020).

[10] T. Dbouk and D. Drikakis, "Weather impact on airborne coronavirus survival," Phys. Fluids **32**, 093312 (2020).

[11] T. Dbouk and D. Drikakis, "On airborne virus transmission in elevators and confined spaces," Phys. Fluids **33**, 011905 (2021).

[12] S. Verma, M. Dhanak, and J. Frankenfield, "Visualizing the effectiveness of face masks in obstructing respiratory jets," Phys. Fluids **32**, 061708 (2020).

[13] P. Prasanna Simha and P. S. Mohan Rao, "Universal trends in human cough airflows at large distances," Phys. Fluids **32**, 081905 (2020).

[14] M.-R. Pendar and J. C. Páscoa, "Numerical modeling of the distribution of virus carrying saliva droplets during sneeze and cough," Phys. Fluids **32**, 083305 (2020).

[15] G. Busco, S. R. Yang, J. Seo, and Y. A. Hassan, "Sneezing and asymptomatic virus transmission," Phys. Fluids **32**, 073309 (2020).

[16] M. Abuhegazy, K. Talaat, O. Anderoglu, and S. V. Poroseva, "Numerical investigation of aerosol transport in a classroom with relevance to Covid-19," Phys. Fluids **32**, 103311 (2020).

[17] T. Dbouk, F. Roger, and D. Drikakis, "Reducing indoor virus transmission using air purifiers," Phys. Fluids **33**, 103301 (2021).

[18] K. Talaat, M. Abuhegazy, O. A. Mahfoze, O. Anderoglu, and S. V. Poroseva, "Simulation of aerosol transmission on a Boeing 737 airplane with intervention measures for COVID-19 mitigation," Phys. Fluids **33**, 033312 (2021).

[19] W. Wang, F. Wang, D. Lai, and Q. Chen, "Evaluation of SARS-CoV-2 transmission and infection in airliner cabins," Indoor Air **32**, e12979 (2022).

[20] F. Wang, T. Zhang, R. You, and Q. Chen, "Evaluation of infection probability of Covid-19 in different types of airliner cabins," Build. Environ. **234**, 110159 (2023).

[21] T. Dbouk and D. Drikakis, "On pollen and airborne virus transmission," Phys. Fluids **32**, 063313 (2020).

[22] S. Bushwick, T. Lewis, and A. Montañez, "Evaluating COVID risk on planes, trains and automobiles," Scientific American (2020).

[23] V. Mathai, A. Das, J. Bailey, and K. Breuer, "Airflows inside passenger cars and implications for airborne disease transmission," Sci. Adv. **7**, eabe0166 (2021).

[24] V. Mathai, A. Das, and K. Breuer, "Aerosol transmission in passenger car cabins: Effects of ventilation configuration and driving speed," Phys. Fluids **34**, 021904 (2022).

[25] K. Luo, Z. Lei, Z. Hai, S. Xiao, J. Rui, H. Yang, X. Jing, H. Wang, Z. Xie, P. Luo, W. Li, Q. Li, H. Tan, Z. Xu, Y. Yang, S. Hu, and T. Chen, "Transmission of SARS-CoV-2 in public transportation vehicles: A case study in Hunan Province, China," Open Forum Infect. Dis. **7**, ofaa430 (2020).

[26]Y. Shen, C. Li, H. Dong, Z. Wang, L. Martinez, Z. Sun, A. Handel, Z. Chen, E. Chen, M. H. Ebell, F. Wang, B. Yi, H. Wang, X. Wang, A. Wang, B. Chen, Y. Qi, L. Liang, Y. Li, F. Ling, J. Chen, and G. Xu, "Community outbreak investigation of SARS-CoV-2 transmission among bus riders in Eastern China," JAMA Intern. Med. **180**, 1665–1671 (2020).
[27]Z. Zhang, T. Han, K. H. Yoo, J. Capecelatro, A. L. Boehman, and K. Maki, "Disease transmission through expiratory aerosols on an urban bus," Phys. Fluids **33**, 015116 (2021).
[28]P. Azimi, Z. Keshavarz, J. Laurent, B. R. Stephens, and J. G. Allen, "Mechanistic transmission modeling of Covid-19 on the Diamond Princess cruise ship demonstrates the importance of aerosol transmission," Proc. Natl Acad. Sci. U. S. A. **118**, e2015482118 (2020).
[29]L. Moriarty, M. Plucinski, B. J. Marston et al., "Public health responses to Covid-19 outbreaks on cruise ships – worldwide, February–March 2020," MMWR Morb. Mortal Wkly Rep. **69**, 347–352 (2020).
[30]E. C. Rosca, C. Heneghan, E. A. Spencer, J. Brassey, A. Plüddemann, I. J. Onakpoya, D. Evans, J. M. Conly, and T. Jefferson, "Transmission of SARS-CoV-2 associated with cruise ship travel: A systematic review," Trop. Med. Infect. Dis. **7**, 290 (2022).
[31]L. Huang, I. Riyadi, S. Utama, M. Li, P. Sun, and G. Thomas, "Covid-19 transmission inside a small passenger vessel: Risks and mitigation," Ocean Eng. **255**, 111486 (2022).
[32]A. Saunders, "Cruise lines change ship ventilation systems as part of overall Covid strategy," Cruise Critic (2020).
[33]K. Wiles, "Cruise ship AC systems could promote rapid coronavirus spread, Prof says," Purdue University News (2020).
[34]O. Almilaji, "Air recirculation role in the spread of COVID-19 onboard the Diamond Princess Cruise ship during a quarantine period," Aerosol Air Qual. Res. **21**, 200495 (2021).
[35]J. Zhou, S. P. Chen, W. W. Shi, M. Kanrak, and J. Ge, "The impacts of COVID-19 on the cruise industry based on an empirical study in China," Mar. Policy **153**, 105631 (2023).
[36]M. Z. Bazant and J. W. M. Bush, "A guideline to limit indoor airborne transmission of COVID-19," Proc. Natl Acad. Sci. U. S. A. **118**, e2018995118 (2021).
[37]CDC. *COVID-19 Ventilation in Buildings 2023* (The Centers for Disease Control and Prevention, 2023).
[38]ASHRAE. *ANSI/ASHRAE Standard 241–2023, Control of Infectious Aerosols* (ASHRAE, 2023).
[39]ASHRAE. *ANSI/ASHRAE Standard 62.1–2019, Ventilation and Acceptable Indoor Air Quality* (ASHRAE, 2019).
[40]WHO. *Roadmap to Improve and Ensure Good Indoor Ventilation in the Context of COVID-19* (World Health Organization, 2021).
[41]REHVA. *COVID-19 Guidance 4.1, How to Operate HVAC and Other Building Service Systems to Prevent the Spread of the Coronavirus (SARS-CoV-2) Disease (COVID-19) in Workplaces* (Federation of European Heating, Ventilation and Air Conditioning Associations, 2021).
[42]Y. Li, P. Cheng, and W. Jia, "Poor ventilation worsens short-range airborne transmission of respiratory infection," Indoor Air **32**, e12946 (2022).
[43]FPS. *Legal Framework Regarding Indoor Air Quality* (Federal Public Service - Public Health, 2022).
[44]J. G. Allen and J. D. Macomber, *Healthy Buildings: How Indoor Spaces Can Make You Sick-Or Keep You Well*, 2nd ed. (Harvard University Press, 2022).
[45]ASHRAE. *ANSI/ASHRAE Standard 62.2–2019, Ventilation and Acceptable Indoor Air Quality in Residential Buildings* (ASHRAE, 2019).
[46]R. Dhand and J. Li, "Coughs and sneezes: Their role in transmission of respiratory viral infections, including SARS-CoV-2," Am. J. Respir. Crit. Care Med. **202**, 651–659 (2020).
[47]M. Zhao, C. Zhou, T. Chan, C. Tu, Y. Liu, and M. Yu, "Assessment of Covid-19 aerosol transmission in a university campus food environment using a numerical method," Geosci. Front. **13**, 101353 (2022).
[48]W. van der Reijden, E. Veerman, and A. Nieuw Amerongen, "Shear rate dependent viscoelastic behavior of human glandular salivas," Biorheology **30**, 141–152 (1993).
[49]B. E. Scharfman, A. H. Techet, J. W. M. Bush, and L. Bourouiba, "Visualization of sneeze ejecta: Steps of fluid fragmentation leading to respiratory droplets," Exp. Fluids **57**, 24 (2016).
[50]S. Zhu, S. Kato, and J. H. Yang, "Study on transport characteristics of saliva droplets produced by coughing in a calm indoor environment," Build. Environ. **41**, 1691–1702 (2006).
[51]X. Xie, Y. Li, H. Sun, and L. Liu, "Exhaled droplets due to talking and coughing," J. R. Soc. Interface **6**, 703–714 (2009).
[52]P. Rosin and E. Rammler, "The laws governing the fineness of powdered coal," J. Inst. Fuel **7**, 29–36 (1933).
[53]W. Weibull, "A statistical distribution function of wide applicability," J. Appl. Mech. **18**, 293–297 (1951).
[54]Y. Liu, Y. Laiguang, Y. Weinong, and L. Feng, "On the size distribution of cloud droplets," Atmos. Res. **35**, 201–216 (1995).
[55]W. E. Ranz and W. R. Marshall, "Evaporation from drops, part I," Chem. Eng. Prog. **48**, 141–146 (1952).
[56]W. E. Ranz and W. R. Marshall, "Evaporation from drops, part II," Chem. Eng. Prog. **48**, 173–180 (1952).
[57]Siemens Digital Industries Software. *Simcenter STAR-CCM+, Version 2210* (Siemens Digital Industries Software, 2022).
[58]L. Schiller and A. Naumann, "Ueber die grundlegenden Berechnungen bei der Schwerkraftaufbereitung," VDI Zeits. **77**, 318–320 (1933).
[59]L. K. Norvihoho, H. Li, Z.-F. Zhou, J. Yin, S.-Y. Chen, D.-Q. Zhu, and B. Chen, "Dispersion of expectorated cough droplets with seasonal influenza in an office," Phys. Fluids **35**, 083302 (2023).
[60]R. C. Reid, J. M. Prausnitz, and B. E. Poling, *The Properties of Gases and Liquids*, 4th ed. (McGraw-Hill, 1987).
[61]R. Bhardwaj and A. Agrawal, "Likelihood of survival of coronavirus in a respiratory droplet deposited on a solid surface," Phys. Fluids **32**, 061704 (2020).
[62]L.-D. Chen, "Effects of ambient temperature and humidity on droplet lifetime – A perspective of exhalation sneeze droplets with Covid-19 virus transmission," Int. J. Hygiene Environ. Health **229**, 113568 (2020).
[63]H. Li, F. Y. Leong, G. Xu, Z. Ge, C. W. Kang, and K. H. Lim, "Dispersion of evaporating cough droplets in tropical outdoor environment," Phys. Fluids **32**, 113301 (2020).
[64]X. Xie, Y. Li, T. Zhang, and H. Fang, "Bacterial survival in evaporating deposited droplets on a Teflon-coated surface," Appl. Microbiol. Biotechnol. **73**, 703–712 (2006).
[65]N. van Doremalen, T. Bushmaker, D. H. Morris, M. G. Holbrook, A. Gamble, B. N. Williamson, A. Tamin, J. L. Harcourt, N. J. Thornburg, S. I. Gerber, J. O. Lloyd-Smith, E. de Wit, and V. J. Munster, "Aerosol and surface stability of HCoV-19 (SARS-CoV-2) compared to SARS-CoV-1," New Engl. J. **382**, 1564–1567 (2020).